Applied Catalysis B: Environmental 221 (2018) 371–379

Contents lists available at ScienceDirect

Applied Catalysis B: Environmental

journal homepage: www.elsevier.com/locate/apcatb

$CuO/ZnO/Ga_2O_3$ catalyst for low temperature MSR reaction: Synthesis, characterization and kinetic model

P. Ribeirinha[a], C. Mateos-Pedrero[a], M. Boaventura[a], J. Sousa[a,b], A. Mendes[a,*]

[a] Laboratório de Engenharia de Processos, Ambiente, Biotecnologia e Energia (LEPABE), Faculdade de Engenharia do Porto, Rua Roberto Frias, 4200-465 Porto, Portugal
[b] Departamento de Química, Escola de Ciências da Vida e do Ambiente, Universidade de Trás-os-Montes e Alto Douro, Quinta de Prados, 5000-801, Vila Real, Portugal

ARTICLE INFO

Keywords:
Methanol steam reforming
Catalyst
Gallium promoted
Hydrogen production
Kinetic model

ABSTRACT

Highly active catalysts for the methanol steam reforming (MSR) capable of operating efficiently at the same temperature of high temperature polymer electrolyte membrane fuel cells (HTPMFCs) devices are strongly desired. A novel $CuO/ZnO/Ga_2O_3$ catalyst was synthesized by co-precipitation method and characterized by ICP-AES, N_2-physisorption, SEM-EDX and XRD. This catalyst showed a catalytic activity 2.2 times higher than commercial $CuO/ZnO/Al_2O_3$ catalysts at 453 K Two kinetic models one empirical and one mechanistic were applied to describe the methanol steam reforming reaction over one of the most promising catalyst family.

1. Introduction

Methanol can be produced from renewable sources, is easy to store and has higher volume energy density than compressed or chemically bonded hydrogen storage technologies [1,2]. Methanol, due to the absence of C—C bonds, has a low reforming temperature (513 K–533 K) [2] making it suitable for fuel cell applications as a hydrogen source. Moreover, the hydrogen-rich gas stream produced by methanol steam reforming (MSR) can be fed directly to high temperature polymer electrolyte membrane fuel cells (HT-PEMFC), due to the high CO tolerance (up to 3 % [3]). However, the low catalytic activity of commercial reforming catalysts at the operating temperatures of HT-PEMFCs (393 K–453 K) [4,5] increases the complexity and reduces the efficiency of power supplies based on HT-PEMFCs integrated with reformers. Thermodynamically, the methanol conversion by MSR reaction is almost complete at 453 K [6], therefore catalysts with high activity at *ca.* 453 K, are conceivable and strongly desired.

Copper-based catalysts, such as $Cu/ZnO/Al_2O_3$, are the most commonly used catalysts for MSR due to their low cost and considerably high activity at temperatures of *ca.* 523 K, despite the pyrophoric nature and low stability [7,8]. The change in oxidation state, reduction of the active area by sintering, coke deposition, catalyst poisoning (*e.g.* chloride and sulphur) are the main reasons for the catalyst deactivation [9,10]. To improve the copper-based catalyst several approaches are reported in literature, from the employment of different preparation methods [11,12] to the addition of promoters [13–16]. The Al_2O_3 is typically used as support and improves the surface area [8]; adding ZrO to Cu-based Al_2O_3 supported, improves the reducibility and copper dispersion [14], while adding CeO has shown to increase the thermal stability and increases the CO conversion through WGS reaction [15,16]. Recently, a gallium-promoted copper-based catalyst prepared by co-precipitation method demonstrated to be highly active, stable and selective at temperatures lower than 473 K [15,17–19]. The incorporation of Ga into the Cu–Zn oxide showed to improve the catalytic activity, by originating a nonstoichiometric cubic spinel phase containing interstitial Cu^{1+} ions, resulting in extremely small (< 5 Å) and highly dispersed copper clusters [17,18].

The search for a more suitable catalyst for MSR has led to consider metals from groups VIII–X due to their high activity, stability and low CO production [20–25]. Pd-based catalysts, for instance display an unusual behaviour since it forms Pd-alloys (*e.g.* Zn and Ga) after proper reductive pre-treatment, modifying the catalytic function of Pd [20–22]. Pt-based catalysts on the other hand demonstrated very high activity; *e.g.* $Pt/In_2O_3/Al_2O_3$ showed an activity 10 times higher than commercial Cu-based catalyst [22–25]. This high activity of $Pt/In_2O_3/Al_2O_3$ has been assigned to the contact regions between the metallic Pt with partially reduced In_2O_3 [25]. The major challenges of using commercially noble metals for MSR is the prohibitive high noble metal loading (typical ranging from 5.0 to 15.0 wt.%), which limits their economic viability.

Kinetic modelling of the methanol steam reforming process is a very important tool for scaling, design and optimize reformers. Several power-law and Langmuir–Hinshelwood reaction rate expressions for MSR over $CuO/ZnO/Al_2O_3$ have been reported in literature, typically for operating temperatures above 473 K [26–31]. In this work two kinetic models, one empirical and one mechanistic are proposed for

* Corresponding author.
E-mail address: mendes@fe.up.pt (A. Mendes).

http://dx.doi.org/10.1016/j.apcatb.2017.09.040
Received 7 July 2017; Received in revised form 5 September 2017; Accepted 16 September 2017
Available online 20 September 2017

characterizing one of the most promising catalyst for MSR, a novel highly active gallium-promoted copper-based catalyst supported on ZnO operating at temperatures between 453 K and 493 K. The CuO/ZnO/Ga_2O_3 catalyst was synthesized *by the co-precipitation method* and characterized concerning the morphology, structure and composition *by ICP-AES, N_2-physisorption, SEM-EDX and XRD*. Additionally, the catalytic activity of the *in*-house catalyst was compared with the one of two commercial catalysts, CuO/ZnO/Al_2O_3 from BASF RP60 (hereafter mentioned as RP60) and from Süd-Chemie G66MR (hereafter mentioned as G66MR). The proposed kinetic models were fitted to the experimental results using a 1D isothermal packed bed reactor simulator.

2. Kinetic models

The kinetic models proposed in this study only consider the MSR reaction (Eq. (1)); water gas shift (WGS, Eq. (2)) and methanol decomposition (MD, Eq. (3)) reactions were not considered due to their very low rates at temperatures below 493 K [32].

$$CH_3OH + H_2O \rightleftarrows CO_2 + 3H_2 \quad \Delta H°_{298K} = +49.7 kJ{\cdot}mol^{-1} \tag{1}$$

$$CO_2 + H_2 \rightleftarrows CO + H_2O \quad \Delta H°_{298K} = +41.2 kJ{\cdot}mol^{-1} \tag{2}$$

$$CH_3OH \rightleftarrows CO + 2H_2 \quad \Delta H°_{298K} = +90.7 kJ{\cdot}mol^{-1} \tag{3}$$

Two types of kinetic models were developed, one empirical (power-law model) and one based on mechanistic assumptions. Empirical models, despite their simplicity, can fit very accurately the experimental results and are easy to implement [30,31]. The mechanistic models, on the other hand, are based on physical assumptions and can express accurately the sequence of the reaction steps for the H_2 formation [26].

2.1. Empirical model

The power-law model expressed by Eq. (4) was adopted in this work to describe the MSR reaction on *in-house* catalyst (CuO/ZnO/Ga_2O_3). The temperature dependence of the reaction rate was assumed to follow an Arrhenius-type behavior (Eq. (5)).

$$r_{MSR} = k_{MSR}(T) p_{CH_3OH}^{a} p_{H_2O}^{b} p_{H_2}^{c} p_{CO_2}^{d} \tag{4}$$

$$k_{MSR}(T) = k_0 e^{-\frac{Ea}{RT}} \tag{5}$$

where, r is the reaction rate of the methanol steam reforming reaction, k is the kinetic constant of the MSR reaction, p are the partial pressures of each component and a, b, c and d are the apparent reaction orders of methanol, water, hydrogen and carbon dioxide, respectively. k_0, is the Arrhenius pre-exponential factor and E_a is the activation energy. The model has a total of 6 parameters, including the activation energy and pre-exponential factor.

2.2. Mechanistic model

The mechanistic model suggested by Peppley et al. [26] to describe the physical processes that occurs in the MSR over the CuO/ZnO/Al_2O_3 catalyst was also considered in this work. The model comprises a set of Langmuir–Hinshelwood rate expressions, similar to those proposed by Jiang et al. [33], which can be describe as follows by Eqs. (6)–(14):

$$S_1 + S_{1a} + CH_3OH\,(g) \underset{k_{-CH_3O^{(1)}}}{\overset{k_{CH_3O^{(1)}}}{\rightleftarrows}} CH_3O^{(1)} + H^{(1a)} \tag{6}$$

$$S_1 + S_{1a} + H_2O\,(g) \underset{k_{-OH^{(1)}}}{\overset{k_{OH^{(1)}}}{\rightleftarrows}} OH^{(1)} + H^{(1a)} \tag{7}$$

$$2S_{1a} + H_2(g) \underset{k_{-H^{(1a)}}}{\overset{k_{H^{(1a)}}}{\rightleftarrows}} 2H^{(1a)} \tag{8}$$

$$CH_3O^{(1)} + S_{1a} \underset{k_{-CH_2O^{(1)}}}{\overset{k_{CH_2O^{(1)}}}{\rightleftarrows}} CH_2O^{(1)} + H^{(1a)} \tag{9}$$

$$CH_3O^{(1)} + CH_2O^{(1)} \underset{k_{-C_2H_5O_2^{(1)}}}{\overset{k_{C_2H_5O_2^{(1)}}}{\rightleftarrows}} CH_3OCH_2O^{(1)} + S_1 \tag{10}$$

$$CH_3OCH_2O^{(1)} + S_{1a} \underset{k_{-CH_3OCHO^{(1)}}}{\overset{k_{CH_3OCHO^{(1)}}}{\rightleftarrows}} CH_3OCHO^{(1)} + H^{(1a)} \tag{11}$$

$$CH_3OCHO^{(1)} + OH^{(1)} \underset{k_{-HCOOH^{(1)}}}{\overset{k_{HCOOH^{(1)}}}{\rightleftarrows}} HCOOH^{(1)} + CH_3O^{(1)} \tag{12}$$

$$HCOOH^{(1)} + S_{1a} \underset{k_{-HCOO^{(1)}}}{\overset{k_{HCOO^{(1)}}}{\rightleftarrows}} HCOO^{(1)} + H^{(1a)} \tag{13}$$

$$HCOO^{(1)} + S_{1a} \underset{k_{-CO_2^{(1)},a}}{\overset{k_{CO_2^{(1)},a}}{\rightleftarrows}} H^{(1a)} + CO_2{}^{(1)} \tag{14}$$

The final rate expression for the MSR reaction is expressed by Eq. (15). Details of the derivation are reported elsewhere [26].

$$r_{MSR} = \frac{\frac{k_{MSR} K^*_{CH_3O^{(1)}} p_{CH_3OH}}{p_{H_2}^{1/2}} \left(1 - \frac{p_{H_2}^3 p_{CO_2}}{k_{MSRP} p_{H_2O} p_{CH_3OH}}\right) C_{S1}^T C_{S1a}^T S_a}{\left(1 + \frac{K^*_{CH_3O^{(1)}} p_{CH_3OH}}{p_{H_2}^{1/2}} + \frac{K^*_{OH^{(1)}} p_{H_2O}}{p_{H_2}^{1/2}} + K^*_{HCOO^{(1)}} p_{H_2}^{1/2} p_{CO_2}\right)\left(1 + \sqrt{K^*_{H^{(1a)}} p_{H_2}}\right)} \tag{15}$$

Eq. (15) considers the adsorption equilibrium constants (K^*_i) for the intermediate species (Eqs. (6)–(14)), the MSR equilibrium constant (K_{MSR}) and the total catalyst surface concentrations of sites 1 (C_{S1}^T) and 2 (C_{S2}^T). The temperature dependence of the kinetic constant was calculated according to the Arrhenius equation (Eq. (5)) and the temperature dependence of the adsorption equilibrium constants was calculated according to van't Hoff equation (Eq. (16)):

$$\ln K_i = \frac{\Delta H}{RT} + \frac{\Delta S}{R} \tag{16}$$

where ΔH and ΔS are the enthalpy and entropy of adsorption respectively. The model has a total of 10 parameters, including the activation energy and pre-exponential factor.

2.3. Parameter estimation

The parameters of the kinetic models (Eqs. (4), (15)) were obtained by non-linear regression method [34,35]. The experimental reaction rates were determined based on the first derivative of the polynomial equation used to fit the experimental methanol conversion as a function of space-time ratio (m_{cat}/F_{MeOH}); the parameters were then obtained minimizing the mean residual sum of the squares (MSRR) of the experimental and model reaction rates. The power-law model has 6 parameters, including the activation energy and pre-exponential factor. According to the values reported in the literature [28–31], the apparent reactions rates were allowed to be any real number between −2 and 2 and the activation energy between 60 and 100 kJ mol^{-1}. The mechanistic model has a total of 10 parameters or 20 when included the temperature dependence, by Arrhenius and by van't Hoff equations.

Following the same strategy reported in literature [27,28,34], the number of parameters was reduced to 6 introducing an initial estimation of the heat of adsorption reported by Skrzypek et al. [29].

2.4. Simulator

The packed bed reactor model was written and implemented using Fortran. The model considers the steady state mass balance equations for each species, the pressure drop, the MSR reaction rates and the respective boundary conditions. The model considers the following simplifications:

- isothermal behavior;
- the gas mixtures follow the ideal gas law;
- no diffusion limitations in the catalyst were considered;
- axially dispersed plug flow with pressure drop described by the Ergun equation,
- negligible radial gradients and uniform cross-sectional void fraction.

Partial mass balance equation:

$$\frac{d}{dz}(up_i) - D_{ax}\frac{d}{dz}\left(P\frac{d}{dz}\left(\frac{p_i}{P}\right)\right) - \frac{m_{cat}}{\varepsilon V}RT\nu_i r_{MSR} = 0 \quad (17)$$

where u is the interstitial velocity, p_i is the partial pressure of species i, D_{ax} is the effective axial dispersion coefficient, P is to total pressure, m_{cat} is catalyst mass, ε is porosity of the catalyst bed, R is the gas constant, ν_i is the stoichiometry coefficient of species i and r_{MSR} is the MSR reaction rate.

Total mass balance equation:

$$\frac{\mathrm{d}}{\mathrm{d}z}(uP) - \frac{m_{cat}}{\varepsilon V}RT\sum \nu_i r_{MSR} = 0 \quad (18)$$

Pressure drop equation:

$$-\frac{dP}{dz} = 150\frac{\mu u}{d_p^2}(1\text{-}\varepsilon)^2 + \frac{7}{4}\frac{\rho_{gas}u^2}{d_p}\frac{(1-\varepsilon)}{\varepsilon} \quad (19)$$

where, Dp is the catalyst diameter, μ is the gas viscosity and ρ_{gas} is the gas density.

2.5. Boundary conditions

- At the reactor's inlet ($z = 0$),

$$D_{ax}\frac{d}{dz}\left(\frac{p_i}{P}\right) = u\frac{p_i - p_i^{\text{inlet}}}{P}, \quad u = u^{inlet} \quad (20)$$

- At the reactor's outlet ($z = 1$),

$$\frac{d}{dz}\left(\frac{p_i}{P}\right) = 0, \quad P = P^{out} \quad (21)$$

The variables present in Eqs. (17)–(21) were converted to dimensionless variables obtaining a new set of equations, which can be found elsewhere [36].

2.6. Numerical solution strategy

To solve the partial differential equations and avoid the numerical instability, an additional time derivative term was added to their right-hand side, transforming the equations into a pseudo-transient problem [36]. The equations were spatially discretized (50 elements) using the finite volumes method. High-resolution schemes (WACEB) were used to calculate the partial pressures of the components [37]. The time integration was carried out using the numerical package developed at the Lawrence Livermore National Laboratory LSODA [38]. The equations were solved until a steady-state solution was reached.

3. Experimental

3.1. Catalyst synthesis and physicochemical characterization

The $CuO/ZnO/Ga_2O_3$ catalyst (65/25/10 wt.%) was prepared by co-precipitation from a 1.1 M aqueous mixture of metal nitrates ($Cu(NO_3)_2$, $Zn(NO_3)_2$ and $Ga(NO_3)_3$), with dropwise addition (0.27–0.64 ml/min) of an aqueous solution of NH_4HCO_3 (1.3 M) under vigorous stirring at fixed conditions of pH (6.5) and temperature (333 K). After 2 h of aging, the resulting precipitate was filtered and thoroughly washed with distilled hot water. The procedure was repeated for several times until the pH value of the filtrate reached the pH of the distilled water. The precipitate was then dried at 383 K overnight and calcined under static air as follows: from 25 K to 473 K (heating rate: 2 K/min; dwell time: 1 h), from 473 K to 633 K (heating rate: 2 K/min; dwell time: 1 h), and finally kept at 633 K for 8.5 h.

The $CuO/ZnO/Ga_2O_3$ catalyst was characterized and evaluated using a variety of methods. The metal content (Cu) was determined from induced coupled plasma (ICP-AES). The morphology and qualitative composition was assessed by scanning electron microscopy equipped with an energy dispersive x-ray high vacuum detector (SEM-EDX). The catalyst surface area was determined by Multi point Brunauer-Emmett-Teller (BET) performed on a Quantachrome Autosorb AS-1 instrument at 77 K. Prior to the analysis the samples were outgassed in vacuum at 473 K for 2 h. The pore size (mesoporosity) was calculated from the N_2-physisorption isotherm using the Barrett-Joyner-Halenda (BJH) method. The porosity and bulk density were determined by mercury porosimetry on Quantachrome Poremaster using a maximum filling pressure of *ca.* 3500 bar. The structure of the catalyst was studied by X-ray powder diffraction (XRD). The XRD pattern of the selected samples was collected using a PANalytical X'Pert Pro operating in Bragg-Bretano focusing geometry and using Cu $K\alpha$ radiation at wavelengths Cu $K\alpha_1$ = 1.5406 Å and Cu $K\alpha_2$ = 1.54443 Å. The data was collected at 2θ angles (20–80°).

3.2. Effect of the particle size on the methanol conversion

Commercial catalyst RP60 ($CuO/ZnO/Al_2O_3$) was used to evaluate the effect of the particle size on the methanol conversion. The catalyst pellets were milled and sieved into particle sizes of 50–150 μm, 100–250 μm, 250–400 μm, 400–600 μm, 600–1000 μm and pellets of 1.5 mm of diameter. The characterization procedure was the same as described below, except that 1.5 g of catalyst was used instead of 0.5 g.

3.3. Kinetic characterization

A differential reactor was filled with 0.5 g of catalyst (*in-house*, RP60 and G66MR catalyst) with particle size ranging between 100 and 250 μm and mixed with 0.5 g of glass beads of the same diameter to achieve near isothermal conditions. The reactor length to catalyst diameter ratio was preserved higher than 50 ($l_{reactor}/d_{particle} \geq 50$) and the reactor diameter to catalyst diameter ratio was higher than 30 ($d_{reactor}/d_{particle} \geq 30$) [39]. Glass wool was inserted in the top and bottom of the reactor to avoid the catalyst particles to be dragged by the stream. During the reduction process the MSR catalysts lose mass and consequently reduce their volume; to avoid channelling the reactor was placed inside the oven in vertical orientation with the temperature being controlled inside the catalyst bed. The catalyst was reduced during 30 min with a mixture of hydrogen, 10 ml/min, and of nitrogen, 190 ml min^{-1}, with a temperature ramp of *ca.* 5 K/min from 433 K to 478 K to avoid sintering the catalyst. The methanol conversion, hydrogen and CO production were accessed between 453 K and 523 K, m_{cat}/F_{MeOH} between 30 kg s mol^{-1} and 550 kg s mol^{-1}, operating pressure between 1 and 3 bar and steam-to-carbon ratio (S/C) of 1:1, 1:1.5, 1:2. The condensable components were removed from the reformate stream using a cold trap, while the non-condensable species

Table 1
Cu content assessed by ICP-AES, BET surface area (sBET) and average pore size (d_p) calculated from N_2 physisorption.

Sample	Cu content (wt.%)	sBET ($m^2\ g^{-1}$)	d_p (nm)	Total Porosity	Bulk Density (kg dm^{-3})
(CuO/ZnO/Ga_2O_3)	51.4	55	19.3	0.54	0.44
G66MR	65 [40]	60 [40]	–	–	1.1

concentration, namely hydrogen and carbon dioxide were determined using a mass spectrometer (Pfeiffer OmniStartm). The CO concentration was determined using a specific analyser (Signal Inst. 7000FM GFC). The performance of the three catalysts was accessed after the activation process (reduction) and after 80 h time-on-stream at 80 % methanol conversion.

4. Results and discussion

4.1. Physicochemical characterization of the in-house catalyst

The physicochemical properties of the in-house catalyst (CuO/ZnO/Ga_2O_3) were characterised using the following techniques: ICP-AES (catalyst composition), N_2-physisorption (BET surface area), mercury porosimetry (porosity), SEM-EDX (structure) and XRD (crystallinity). The metal content (Cu) of the *in-house* catalyst obtained by ICP is shown in Table 1; the Cu content (51.4 wt.%) is close to the nominal content (52 wt.%), indicating that the preparation method was adequate. The highest catalytic activity reported in literature for this family of catalyst was achieved for a Cu atomic content of 43 % [17,18]. Increasing the Cu content by reducing the Ga content originates a negligible loss in catalytic activity [17], but represents an important reduction in the catalyst cost. Commercial CuO/ZnO/Al_2O_3 catalysts normally presents a Cu atomic content of *ca.* 65 wt.% [40]. The BET surface area of the CuO/ZnO/Ga_2O_3 catalyst was 55 $m^2\ g^{-1}$, which is in line to the surface area obtained by Tong et al. [17] for its most active catalysts, but it is lower than the surface area of the of commercial catalyst G66MR, *ca.* 60 $m^2\ g^{-1}$ [40]. The CuO/ZnO/Ga_2O_3 porosity and bulk density obtained by mercury porosimetry were 0.54 and 0.44 kg dm^{-3}, respectively. The bulk density of the in-house is quite low; commercial catalysts are typically pelletized at high pressures in the presence of binders, which increases significantly the density. This is the case of catalyst commercial G66MR, which shows a density of 1.1 kg dm^{-3} according to the manufacturing.

The structure of the CuO/ZnO/Ga_2O_3 catalyst, after calcination and reductive treatment with H_2 was studied by XRD; the results are shown in Fig. 1. The XRD patterns of the calcined CuO/ZnO/Ga_2O_3 sample

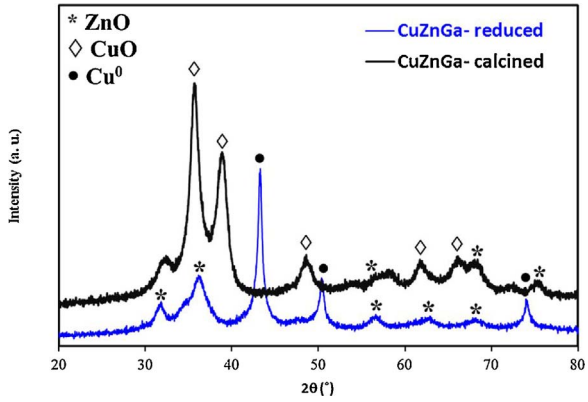

Fig. 1. XRD patterns of the CuO/ZnO/Ga_2O_3 sample after calcination in air at 633 K for 8.5 h (CuO/ZnO/Ga_2O_3-calcined) and reduced in H_2 at 478 K for 30 min (CuO/ZnO/Ga_2O_3-reduced).

exhibit the main lines of CuO (JCPDS file no. 48–1548) at 35.5° (11-1) and 38.7° (111) with some minor and broad reflections at 31.7° and 36.8° corresponding to (100) and (101) planes of ZnO (JCPDS file no. 36–1451). The XRD pattern (Fig. 1) of the reduced catalyst shows peaks at 43.5° Cu(111), 50.3° Cu(200) and 74.3° Cu(220) ascribed to Cu^0 (JCPDS file no. 04-0836). As for the calcined sample, the peaks of ZnO are also observed. It is clear in this figure that after reduction the peaks became sharper and narrower, characteristic of a high crystallinity. XRD patterns of the calcined and reduced CuZnGa catalysts in this study did not show any peak characteristic of crystalline Ga phases, suggesting that Ga particles are very small and highly dispersed. This was reported for CuZnGa catalysts with similar composition [41] and for Ga doped CuZn samples where the formation of a $ZnGa_2O_4$ phase appears to depend on the calcination temperature and sample composition [42]. The absence of Ga peaks suggests that Ga particles are very small and highly dispersed. SEM-EDS results (Fig. 2) show Cu, Zn and elements homogeneously distributed on the catalysts surface.

4.2. Catalyst particle size effect, diffusion limitations

It is well known that the mass transport of reagents from the bulk to the catalyst active sites, may play an important effect on the rate of the reaction [43]. To compare catalyst and obtain the correct kinetic rate parameters, the size of the catalyst particles was reduced to a size were the diffusion control limitations were virtually eliminated. Small amounts of the *in-house* catalyst were produced in each batch, therefore to perform this experiments the commercial RP60 catalyst was used, since a large quantity of catalyst was required. Fig. 3 shows the methanol conversion as a function of space-time ratio for different catalyst particle sizes at 453 K, 473 and 493 K using a RP60 catalyst. At temperature of 453 K, the effect of the particle size on the methanol conversion is negligible, gaining only importance for space-time ratios higher than 300 kg s mol^{-1}, when small particle sizes show high methanol conversions. For sizes smaller than 100 μm it is observed an inversion of this trend; very small particle sizes (powders) originate flow-channelling that decreases the methanol conversion. Particle sizes between 100 μm and 250 μm show high methanol conversions for all tested space-time ratios and temperatures. The kinetics of the reaction at low space-time ratios and low temperature is rate limited, moving for diffusional control as the temperature and/or space-time ratio increases [43]; in the case of small particle sizes the diffusional control occurs at higher temperatures and higher space-time ratios when compared to larger catalyst particles. Lee et al. [28] observed no intraparticle diffusion limitations at temperatures below 473 K for particle size ranging between 300 μm–400 μm using a commercial catalyst, and Agrell et al. [44] concluded that only at temperatures above 493 K diffusion limitations are observed for a particle size between 120 μm and 250 μm. The smaller catalyst particles originate higher methanol conversions, but can also originate higher pressure drops; for small size reformers, however, pressure drop is not a limitation.

4.3. Methanol and CO production of In-house and commercial catalysts

The reduction of the catalysts (activation process) is an exothermic process that influences the catalyst ability to perform the methanol steam reforming reaction. The catalyst reduction with hydrogen at high temperatures such as 513 K is a very fast process that may sinter the catalyst due to the heat released in the process. Small particles of catalyst are more prone of sintering than pellets, therefore, the reduction process was performed using hydrogen diluted with nitrogen (1:9 v/v) at low temperatures (< 478 K). Fig. 4 shows the methanol conversion as a function of the space-time ratio immediately after activation for the *in-house* catalyst (CuO/ZnO/Ga_2O_3) and commercial catalysts G66MR and RP-60 (CuO/ZnO/Al_2O_3). The two commercial catalysts present similar performances at 453 K, while the in-house catalyst shows clearly a higher performance. The methodology reported in the

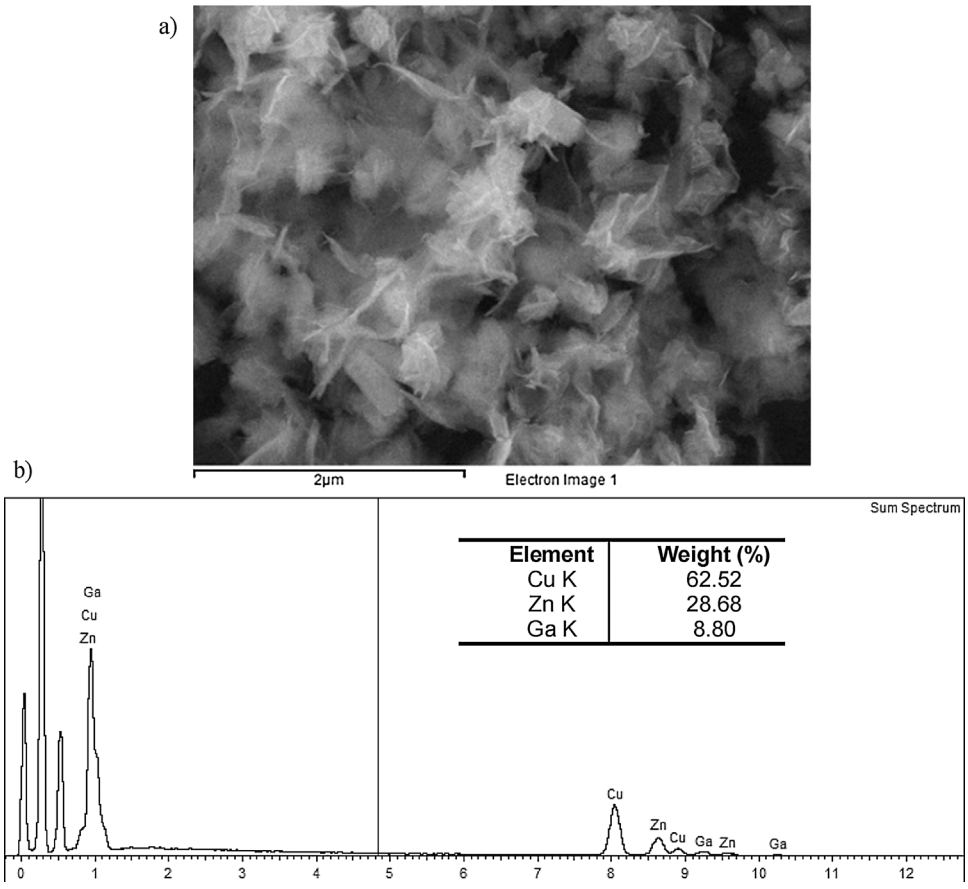

Fig. 2. SEM image (a) and EDS results (b) of the $CuO/ZnO/Ga_2O_3$ catalyst.

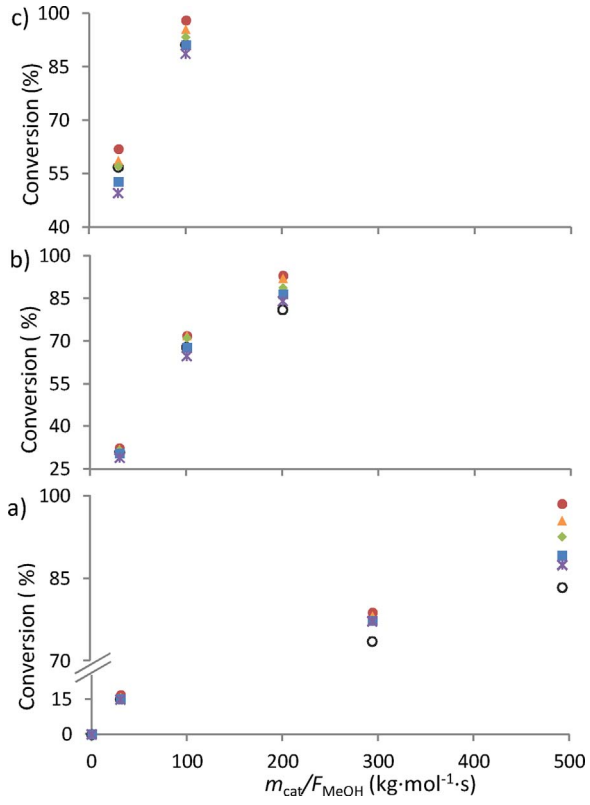

Fig. 3. Catalyst (RP60) particle size effect on the methanol conversion at 453 K (a), 473 K (b) and 493 K (c), P = 1 bar, and S/C = 1.5. 0–100 μm (○); 100–250 μm (●); 250–400 μm (▲); 400-600 μm (♦); 600–1000 μm (■); pellets (✳).

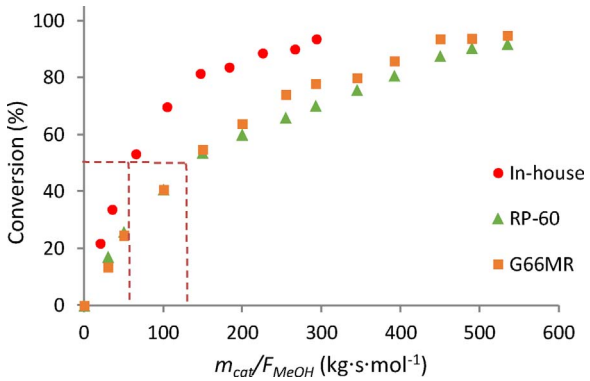

Fig. 4. Methanol conversion as function of the space-time ratio, for the in-house, G66MR and RP-60 catalysts, at 453 K, P = 1 bar, S/C = 1.5 and particle size of 100–250 μm.

literature to compare catalyst activities is not consensual [17,23]; in this study, the activity was compared based on the space-time ratio required to achieve 50 % of methanol conversion. The in-house catalyst presents between 2.2 and 2.3 times higher activity than G66MR and RP-60, since it achieves 50 % of methanol conversion at a m_{cat}/F_{MeoH} of *ca.* 60 kg s mol^{-1}, while the commercial catalysts achieve the same methanol conversion at 130–140 kg s mol^{-1}. The $CuO/ZnO/Ga_2O_3$ exhibited a catalytic activity similar to the one reported in literature for this catalyst family [17–19]. Using a $CuO/ZnO/Ga_x$ with an atomic content of 48.7% of Cu, 31.3% of Zn and 20% of Ga, Tong et al. [17] reported a methanol conversion of 33% at 468 K and m_{cat}/F_{MeoH} of 18 kg s mol^{-1}m, while in this work the conversion for the same operating condition s was 37%. Lotric et al. [19] using a $CuZnGaO_x$ catalyst with the molar ratio of 5:3:2: (Cu:Zn:Ga) reported 80 % of methanol conversion at 453 K and m_{cat}/F_{MeoH} of 150 kg s mol^{-1}; similar

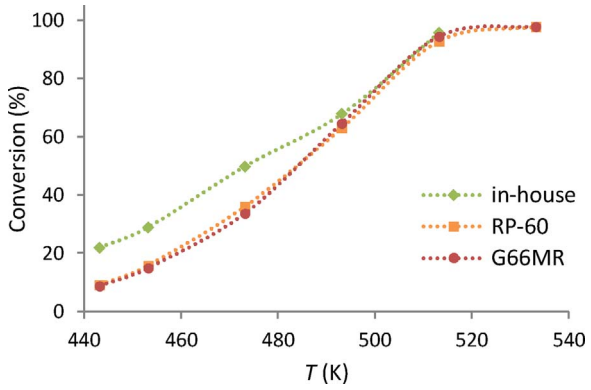

Fig. 5. Methanol conversion as function of temperature for the in-house, G66MR and RP-60 catalysts, at m_{cat}/F_{MeOH} = 30 kg s mol^{-1}, P = 1 bar, S/C = 1.5 and particle size of 100–250 μm. Lines were added for readability.

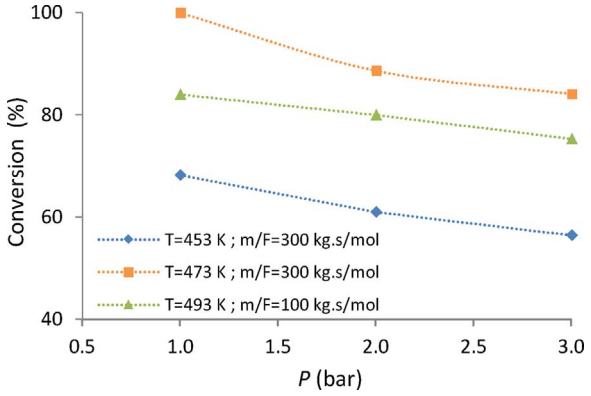

Fig. 7. Methanol conversion as a function of pressure using RP60 catalyst, at 453 K, m_{cat}/F_{MeOH} = 300 kg s mol^{-1}, S/C = 1.5 and particle size of 100–250 μm.

conversion is depicted in Fig. 4 for the same space-time ratio. Fig. 5 shows the methanol conversion as a function of the temperature for the three catalysts. The in-house catalyst shows a higher performance than the commercial ones at low temperature; at 443 K the in-house catalyst has a methanol conversion of ca. 22%, while the commercial catalyst is less than 9%. Above 493 K all the catalyst shows similar methanol conversions. This similar performance may be attributed to the reduction of the active area due to sintering of the small Cu nanoparticles leading to an irreversible performance loss.

The CO content at 453 K is low for all the tested catalyst reaching a maximum of *ca.* 2000 ppm, when all methanol is converted (Fig. 6). At this operating temperature the carbon monoxide production comes almost exclusively from the RWGS. Therefore, the CO concentration increases with the hydrogen and carbon dioxide partial pressures, that increases with the space-time ratio (m_{cat}/F_{MeOH}). It is also clear from Fig. 6, that the in-house catalyst does not promote the CO production; e.g. at 80% of methanol conversion the CO content in the reformate stream is ca. 600 ppm, while the commercial catalysts has a CO content of ca. 1700 ppm. For HT-PEMFC applications, which is the goal of this work, the CO tolerance is up 30 000 ppm [3], therefore the methanol conversion at low temperatures is a more critical subject that the CO production. On the other hand, for automotive application using low-temperature PEMFC the CO content in hydrogen stream should be less than 0.2 ppm, according to ISO/TS 14687-2 [45], reinforcing the need of highly active MSR catalyst operating at temperatures lower than 423 K.

The effect of the total operating pressure on the methanol conversion was addressed, as depicted in Fig. 7. The decrease of the methanol conversion with the total pressure increase is noticeable for all studied temperatures and space-time ratios. In fact, the principle of Le Chatelier states that with a total pressure increase, the side of the equilibrium with smaller number of moles is more favourable. The kinetic model developed by Peppley et al. [26] for the methanol steam reforming (MSR) using a $CuO/ZnO/Al_2O_3$ catalyst (BASF K3-110) also predicts that increasing pressure would favour the reverse reaction, leading to a decrease of the overall reaction rate. No significant benefit is disclosed of operating at high pressure, except when the reformate is directly fed to a high temperature polymer electrolyte membrane fuel cell (HT-PEMFC). Waller et al. [46] concluded that the performance losses in the fuel cell due to the anode feed dilution could be overcome through increasing the operating pressure and/or temperature within reasonable limits.

The steam-to-carbon ratio can influence the methanol conversion, but also represents an energy cost due to water vaporization. Fig. 8 shows the methanol conversion as a function of the steam-to-carbon ratio, at 453 K. An increase of the methanol conversion is observed when the steam-to-carbon ratio varies from 1 to 2 while a further increase has no significant effect. Considering the energy costs of water vaporization in a HT-PEMFC integrated with a reformer, steam-to-carbon ratio above 2 are questionable.

The catalytic activity decreases after a few hours of operation levelling out afterwards; it is therefore important to access the catalysts deactivation and the catalysts performance at the steady state. Starting with the same methanol conversion for the tested catalysts, *ca.* 80% (space-time ratio of 300 kg s mol^{-1} for commercial catalysts and 150 kg s mol^{-1} for the *in*-house catalyst) the reaction was left running during *ca.* 80 h (time-on-stream) at 453 K (Fig. 9). The commercial catalyst RP60 shows to be the most stable catalyst with a conversion loss of six percentage points, while the in-house catalyst shows *ca.* twenty percentage points of conversion loss. Again, this higher conversion loss of the in-house catalyst should be assigned to the

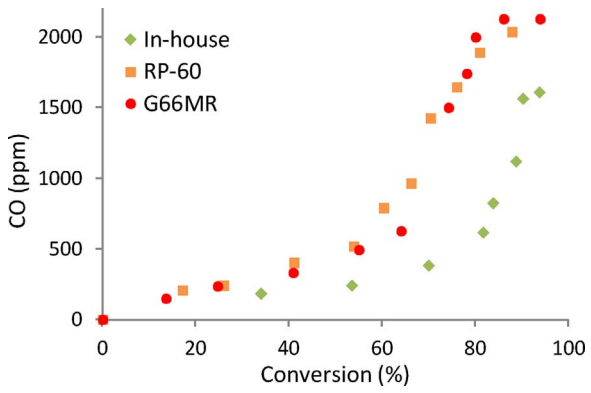

Fig. 6. CO production as function of methanol conversion for the in-house, G66MR and RP-60 catalysts, at 453 K, P = 1 bar, S/C = 1.5 and particle size of 100–250 μm.

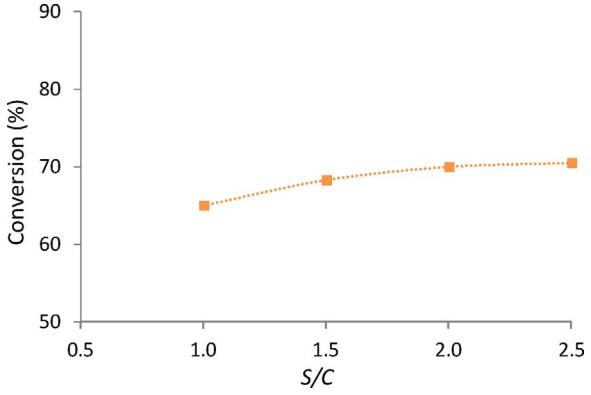

Fig. 8. Methanol conversion as a function of steam-to-carbon ratio using RP60 catalyst at 453 K, m_{cat}/F_{MeOH} = 300 kg s mol^{-1}, P = 1 bar and particle size of 100–250 μm.

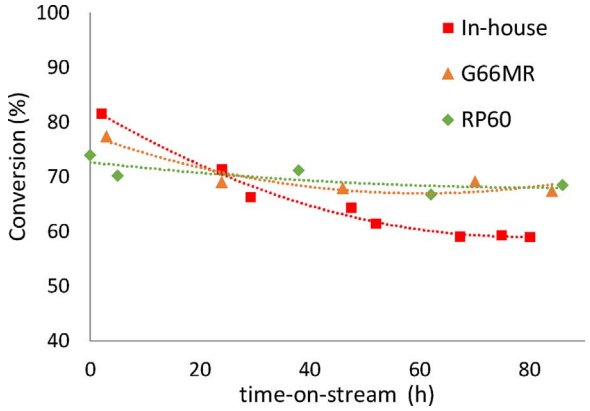

Fig. 9. Conversion as a function of the time for *in-house*, G66MR and RP-60 catalysts, at 453 K, P = 1 bar, S/C = 1.5 and particle size of 100-250 μm.

agglomeration of the very small copper clusters (sintering), which reduces the active surface area, and also due to partial oxidation of the cooper particles [47]. Also, the noticeable fragmentation of the fragile catalyst particles inside the reactor may cause flow channelling and then loss of conversion.

Fig. 10 shows the methanol conversion as a function of the space-time ratio at 453 K for the different catalysts after 80 h of operation. Despite a considerable loss in performance, the in-house catalyst still shows higher performance than the commercial catalysts. The CuO/ZnO/Ga_2O_3 achieves 50 % of methanol conversion at a space-time ratio of *ca.* 95 kg s mol^{-1}, while the commercial catalysts reach this methanol conversion value at *ca.* 160 kg s mol^{-1}. These results indicate an in-house catalyst activity 1.7 times higher than the commercial catalysts. After 80 h of operation both commercial catalysts present equal performance in all the tested range of temperatures and space-time ratio.

4.4. Kinetic models, in-house catalyst

For the commercial catalysts such as RP60 or G66MR several mechanistic and empirical kinetic models can be found in literature [27,34]. However, only Lotric et al. [19] presented a power-law empirical relation to describe the reaction kinetics of the MSR reaction over the catalyst CuO/ZnO/Ga_2O_3. Moreover, that model [19] was developed considering the initial activity of the catalyst, neglecting the deactivation observed for this type of catalyst. The estimated parameters for the power-law and mechanistic models were obtained after stabilization of the catalytic activity of the in-house catalyst and are reported in Table 2. The goodness of the fitting was assessed using parity plots and the models predictions were compared with the experimental data. As previously mentioned, the variables present in Eqs.

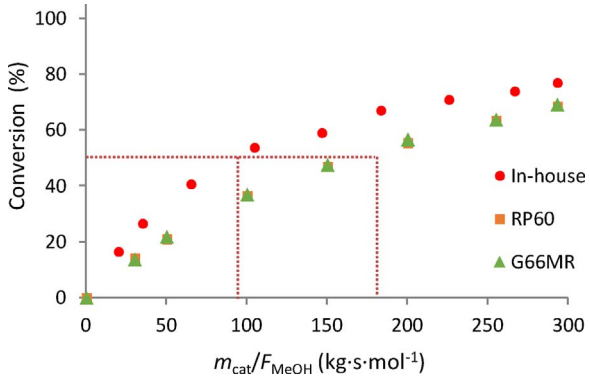

Fig. 10. Methanol conversion as function of the space-time ratio, for *in-house*, G66MR and RP-60 catalysts, at 453 K, P = 1 bar, S/C = 1.5 and particle size of 100-250 μm.

Table 2
Estimated parameters for the power-law and mechanistic model.

Parameter		Power-law model	Mechanistic model
k_0		8.51 × 10^8 (mol kg^{-1} s $bar^{-1.72}$)	7.1 × 10^{10} (mol kg^{-1} s^{-1})
E_a (kJ mol^{-1})		90.8	103.2
a		0.37	–
b		1.35	–
c		0	–
d		0	–
$K^*_{CH3O(1)}$ ($bar^{-0.5}$)	ΔH°_{298} (kJ mol^{-1})	–	−18.8
	ΔS°_{298} (J mol^{-1} K^{-1})	–	−55.4
$K^*_{OH(1)}$ ($bar^{-0.5}$)	ΔH°_{298} (kJ mol^{-1})	–	−17.3
	ΔS°_{298} (J mol^{-1} K^{-1})	–	−43.8
$K^*_{H(1a)}$ ($bar^{-0.5}$)	ΔH°_{298} (kJ mol^{-1})	–	−57.4
	ΔS°_{298} (J mol^{-1} K^{-1})	–	−154.2
$K^*_{HCOO(1)}$ ($bar^{-0.5}$)	ΔH°_{298} (kJ mol^{-1})	–	128.3
	ΔS°_{298} (J mol^{-1} K^{-1})	–	84.6

(17)–(21) were converted to dimensionless variables, where the effective were axial dispersion coefficient (Dax) was replaced by the dimensionless Peclet number. According to the literature, for the operating conditions considered in this work, the Peclet number should assume a large value (> 100), since the axial dispersion in the reactor channel is negligible and the flow in the channel is close to plug flow [34,35].The parameter and operating conditions used for the simulations are presented in Table 3.

The calculated and experimental reaction rates using the power-law model present a good fitting, as shown in the parity plot (Fig. 11a), with a MRSS = 2.8 × 10^{-6}. The simulation results using the power-law model, despite its simplicity, shows a good agreement with the experimental data for the studied conditions, as depicted in Fig. 11b; the maximum relative difference between experimental and simulated results is less than 8% (at 493 K) and the coefficient of determination (R^2) is > 0.97. The obtained power-law model assumes a zero order apparent reaction for hydrogen and carbon dioxide (Table 2). Several authors also reported In the literature apparent reaction of zero order for hydrogen and carbon dioxide using power-law models to predict the methanol conversion of different *in*-house and commercial catalysts [19,34,40]. However, it is well-known that the partial pressures of hydrogen and carbon dioxide affect the MSR reaction rate [26–28]. This inability to describe correctly the reaction rates highlights the limitations of power-law models and emphasizes the need of mechanistic models. The mechanistic model also displays a good fitting between the calculated and experimental reaction rates (Fig. 11c) with a MRSS = 3.2 × 10^{-6}. In general, the obtained parameters are similar to

Table 3
Parameter used in the simulation.

Property	Value
Bulk density (kg m^{-3})	0.44
Porosity	0.54
Particle size (μm)	100–250
Temperature (K)	453–493
S/C	1.5
Pressure (bar)	1

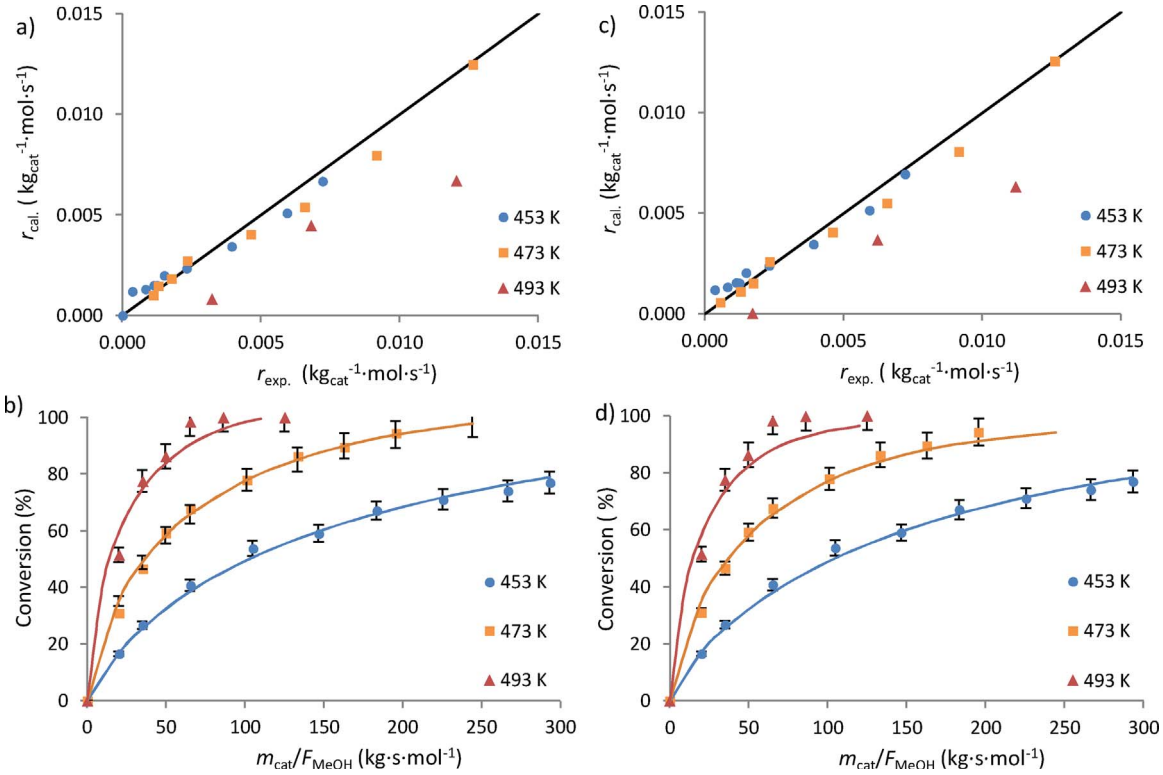

Fig. 11. Parity plot of the experimental and calculated methanol consumption rate using the power-law model (a) and the mechanistic model (c). Experimental (symbols) and simulated (lines) results of methanol conversion as a function of space-time ratio and for different temperatures, using the power-law model (b) and mechanistic model (d).

those reported in literature for the same mechanistic model [26,34]. The main difference is related to the MSR reaction rate (k_{MSR}); Peppley et al. [26] reported for the commercial catalyst BASF K3-110 almost the same value for the activation energy, *ca.*103 kJ mol^{-1} vs 103.2 kJ mol^{-1} in this work, but a lower k_0, *ca.* 8 × 10^9 mol kg^{-1} s^{-1} vs 7.1 × 10^{10} mol kg^{-1} s^{-1} in this work. Silva et al. [40] reported for the commercial catalyst G66MR a MSR reaction rate of 0.025 mol kg^{-1} s^{-1} at 453 K, while in this work and for the same temperature the MSR reaction rate obtained was 0.090 mol kg^{-1} s^{-1}. Fig. 11d shows the simulator predictions using the mechanistic model and experimental results for the methanol conversion. A good agreement to the experimental data for the studied conditions is observed; the maximum relative difference between experimental and simulated results is less than 10 % and the coefficient of determination (R^2) is > 0.97. Both model shows high accuracy and can be used for scaling, design and optimize reformers for the HT-PEMFC applications.

5. Conclusions

A highly active CuO/ZnO/Ga_2O_3 was synthesized by co-precipitation method. The developed catalyst was characterized concerning morphology, structure and composition. The physicochemical study conducted over the *in*-house CuO/ZnO/Ga_2O_3 indicates that the preparation method was adequate for providing very small and highly dispersed copper particles. The performance of the developed catalyst was compared to two commercial CuO/ZnO/Al_2O_3 catalysts, BASF RP60 and Sud-Chemie G66MR, using a tubular MSR reactor. Catalyst particles size ranging between 100 and 250 μm were found to maximize the methanol conversion. Increasing the operating pressure above 1 bar was found to be detrimental for the methanol conversion and no significant gain is observed for values of steam-to-carbon ratio above 2. In-house CuO/ZnO/Ga_2O_3 catalyst immediately after the activation shows a methanol conversion *of ca.* 2.2 times higher than BASF RP60 and Sud-Chemie G66MR, levelling out to *ca.* 1.7 times after 80 h of time-on-stream. The two kinetic models, a power-law and mechanistic, were used to describe the methanol steam reforming reaction over a novel *in-house* catalyst. After proper parameter estimation, the two models were validated using a packed bed reactor simulator, showing for both cases a good agreement between the predicted and experimental methanol conversions.

Acknowledgements

P. Ribeirinha and C. Mateos-Pedrero acknowledge FCT (Grants PD/BD/52621/2014 and SFRH/BPD/97114/2013). The authors would like to thank the European Union's Seventh Framework Programme (FP7/2007-2013) for the FCH JU under GA 303476 due to the funding received for part of this work (www.beingenergy.eu). This work was partially supported by the Projects − POCI-01-0145-FEDER-006939 (Laboratory for Process Engineering, Environment, Biotechnology and Energy − UID/EQU/00511/2013) funded by the European Regional Development Fund (ERDF), through COMPETE2020 − Programa Operacional Competitividade e Internacionalização (POCI) and by national funds, through FCT − Fundação para a Ciência e a Tecnologia and NORTE-01-0145-FEDER-000005-LEPABE-2-ECO-INNOVATION, supported by North Portugal Regional Operational Programme (NORTE 2020), under the Portugal 2020 Partnership Agreement, through the European Regional Development Fund (ERDF).

References

[1] M. Conte, Energy | Hydrogen Economy, Encyclopedia of Electrochemical Power Sources, (2009), pp. 232–254.
[2] S. Sá, H. Silva, L. Brandão, J.M. Sousa, A. Mendes, Catalysts for methanol steam reforming—A review, Appl. Catal. B: Environ. 99 (2010) 43–57.
[3] S.K. Das, A. Reis, K.J. Berry, Experimental evaluation of CO poisoning on the performance of a high temperature proton exchange membrane fuel cell, J. Power Sources 193 (2009) 691–698.
[4] G. Schuller, F. Vázquez, W. Waiblinger, S. Auvinen, P. Ribeirinha, Heat and fuel coupled operation of a high temperature polymer electrolyte fuel cell with a heat exchanger methanol steam reformer, J. Power Sources 347 (2017) 47–56.
[5] S.L. Sahlin, S.J. Andreasen, S.K. Kær, System model development for a methanol

reformed 5 kW high temperature PEM fuel cell system, Int. J. Hydrogen Energy 40 (2015) 13080–13089.
[6] J.C. Amphlett, M.J. Evans, R.A. Jones, R.F. Mann, R.D. Weir, Hydrogen production by the catalytic steam reforming of methanol part 1: The thermodynamics, Can. J. Chem. Eng. 59 (1981) 720–727.
[7] D.R. Palo, R.A. Dagle, J.D. Holladay, Methanol steam reforming for hydrogen production, Chem. Rev. 107 (2007) 3992–4021.
[8] M.B. Fichtl, D. Schlereth, N. Jacobsen, I. Kasatkin, J. Schumannd, M. Behrensd, et al., Kinetics of deactivation on Cu/ZnO/Al2O3 methanol synthesis catalysts, Appl. Catal. A: Gen. 502 (2015) 262–270.
[9] H.H. Kung, Deactivation of methanol synthesis catalysts − a review, Catal. Today 11 (4) (1992) 443–453.
[10] M.V. Twigg, M.S. Spencer, Deactivation of copper metal catalysts for methanol decomposition, methanol steam reforming and methanol synthesis, Top. Catal. 22 (2003) 191–203.
[11] J.-P. Shen, C. Song, Influence of preparation method on performance of Cu/Zn-based catalysts for low-temperature steam reforming and oxidative steam reforming of methanol for H2 production for fuel cells, Catal. Today 77 (2002) 89–98.
[12] C.-Z. Yao, L.-C. Wang, Y.-M. Liu, Gi-S Wu, Y. Cao, W.-L. Dai, et al, Effect of preparation method on the hydrogen production from methanol steam reforming over binary Cu/ZrO2 catalysts, Appl. Catal. A: Gen. 297 (2006) 151–158.
[13] R.O. Idem, N.N. Bakhshi, Production of hydrogen from methanol over promoted coprecipitated Cu-Al catalysts: the effects of various promoters and catalyst activation methods, Ind. Eng. Chem. Res. 34 (1995) 1548–1557.
[14] L. Yong-Feng, D. Xin-Fa, L. Wei-Ming, Effects of ZrO2-promoter on catalytic performance of CuZnAlO catalysts for production of hydrogen by steam reforming of methanol, Int. J. Hydrogen Energy 29 (2004) 1617–1621.
[15] A. Pohar, S. Hŏcevar, B. Likozar, J. Levec, Synthesis and characterization of gallium-promoted copper-ceriacatalyst and its application for methanol steam reforming in a packed bed reactor, Catal. Today 256 (2015) 358–364.
[16] X. Zhang, P. Shi, Production of hydrogen by steam reforming of methanol on CeO2 promoted Cu/Al2O3 catalysts, J. Mol. Catal. A Chem. 194 (2003) 99–105.
[17] W. Tong, A. West, K. Cheung, K.-M. Yu, S.C.E. Tsang, Dramatic effects of gallium promotion on methanol steam reforming cu-ZnO catalyst for hydrogen production: formation of 5 Å copper clusters from Cu-ZnGaOx, ACS Catal. 3 (2013) 1231–1244.
[18] K.M.K. Yu, W. Tong, A. West, K. Cheung, T. Li, G. Smith, et al., Non-syngas direct steam reforming of methanol to hydrogen and carbon dioxide at low temperature, Nat. Commun. 3 (2012) 1230.
[19] A. Lotric, M. Sekavcnik, A. Pohar, B. Likozar, S. Hocevar, Conceptual design of an integrated thermally self-sustained methanol steam reformer e High-temperature PEM fuel cell stack manportable power generator, Int. J. Hydrogen Energy 42 (2017) 16700–16713.
[20] C.S.R. Azenha, C. Mateos-Pedrero, S. Queirós, P. Concepción, A. Mendes, Innovative ZrO2-supported CuPd catalysts for the selective production of hydrogen from methanol steam reforming, Appl. Catal. B: Environ. 203 (l) (2017) 400–407.
[21] K.M. Eblagon, P.H. Concepción, H. Silva, A. Mendes, Ultraselective low temperature steam reforming of methanol over PdZn/ZnO catalysts—Influence of induced support defects on catalytic performance, Appl. Catal. B: Environ. 154–155 (2014) 316–328.
[22] N. Iwasa, N. Takezawa, New supported Pd and Pt alloy catalysts for steam reforming and dehydrogenation of methanol, Top. Catal. 22 (2003) 215–224.
[23] G. Kolb, S. Keller, S. Pecov, H. Pennemann, R. Zapf, Development of micro-structured catalytic wall reactors for hydrogen production by methanol steam reforming over novel Pt/In2O3/Al2O3 catalysts, Chem. Eng. Trans. 24 (2011) 133–138.
[24] G. Kolb, S. Keller, D. Tiemann, K.-P. Schelhaas, J. Schürer, O. Wiborg, Design and operation of a compact microchannel 5kWel: net methanol steam reformer with novel Pt/In2O3 catalyst for fuel cell applications, Chem. Eng. J. 207–208 (2012) 388–402.
[25] R.L. Barbosa, V. Papaefthimiou, Y.T. Law, D. Teschner, M. Hävecker, A. Knop-Gericke, et al., Methanol steam reforming over indium-promoted Pt/Al2O3 catalyst: nature of the active surface, J. Phys. Chem. C 117 (2013) 6143–6150.
[26] B.A. Peppley, J.C. Amphlett, L.M. Kearns, R.F. Mann, Methanol steam reforming on Cu/ZnO/Al2O3 catalysts. Part 2: a comprehensive kinetic model, Appl. Catal., A 179 (1999) 31–49.
[27] P. Ribeirinha, M. Abdollahzadeh, M. Boaventura, A. Mendes, H2 production with low carbon content via MSR in packed bed membrane reactors for high-temperature polymeric electrolyte membrane fuel cell, Appl. Energy 188 (2017) 409–419.
[28] J.K. Lee, J.B. Ko, D.H. Kim, Methanol steam reforming over Cu/ZnO/Al2O3 catalyst: kinetics and effectiveness factor, Appl. Catal. A: Gen. 278 (2004) 25–35.
[29] Skrzypek, J. Sloczynski, S. Ledakowicz, Methanol Synthesis, Polish Scientific Publishers, Warsaw, 1994 ISBN 83–01-11490–8.
[30] P. Ribeirinha, M. Boaventura, José Carlos B. Lopes, José M. Sousa, A. Mendes, Study of different designs of methanol steam reformers: experiment and modelling, Int. J. Hydrogen Energy 39 (2014) 19970–19981.
[31] K. Kobl, S. Thomas, Y. Zimmermann, K. Parkhomenko, A.-C. Roger, Power-law kinetics of methanol synthesis from carbon dioxide and hydrogen on copper-zinc oxide catalysts with alumina or zirconia supports, Catal. Today 270 (2016) 31–42.
[32] H. Purnama, T. Ressler, R.E. Jentoft, H. Soerijanto, R. Schlögl, R. Schomäcker, CO formation/selectivity for steam reforming of methanol with a commercial CuO/ZnO/Al2O3 catalyst, Appl. Catal. A: Gen. 259 (2004) 83–94.
[33] C.J. Jiang, D.L. Trimm, M.S. Wainwright, N.W. Cant, Kinetic mechanism for the reaction between methanol and water over a Cu-ZnO-Al2O3 catalyst, Appl. Catal. A: Gen. 97 (1993) 145–158.
[34] S. Sá, J.M. Sousa, A. Mendes, Steam reforming of methanol over a CuO/ZnO/Al2O3 catalyst, part I: Kinetic modelling, Chem. Eng. Sci. 66 (2011) 4913–4921.
[35] C. Cao, G. Xia, J. Holladay, E. Jones, Y. Wang, Kinetic studies of methanol steam reforming over Pd/ZnO catalyst using a microchannel reactor, Appl. Catal. A: Gen. 262 (1) (2004) 19–29.
[36] S. Sá, H. Silva, J.M. Sousa, A. Mendes, Hydrogen production by methanol steam reforming in a membrane reactor: palladium vs carbon molecular sieve membranes, J. Membr. Sci. 339 (2009) 160–170.
[37] B. Song, G.R. Liu, K.Y. Lam, R.S. Amano, On a higher-order bounded discretization scheme, Int. J. Numer. Methods Fluids 32 (2000) 881–897.
[38] L. Petzold, Automatic selection of methods for solving stiff and nonstiff systems of ordinary differential equations, SIAM J. Sci. Stat. Comput. 4 (1983) 136–148.
[39] G.F. Froment, K.B. Bischoff, Chemical Reactor Analysis and Design, Wiley, New York, 1990.
[40] H. Silva, C. Mateos-Pedrero, P. Ribeirinha, M. Boaventura, A. Mendes, Low-temperature methanol steam reforming kinetics over a novel CuZrDyAl catalyst, Reaction Kinetics, Mech. Catal. 115 (2115) (2017) 321–339.
[41] X. Liu, J. Toyir, P.R. de la Piscina, N. Homs, Hydrogen production from methanol steam reforming over Al_2O_3- and ZrO_2-modified $CuOZnOGa_2O_3$ catalysts, Int. J. Hydrogen Energy 42 (19) (2017) 13704–13711.
[42] M.M.-J. Li, J. Zheng, J. Qu, F. Liao, E. Raine, W.C.H. Kuo, et al., The remarkable activity and stability of a highly dispersive beta-brass Cu-Zn catalyst for the production of ethylene glycol, Nat.: Sci. Rep. 6 (2016) 20527.
[43] H. Scott, Fogler, Elements of Chemical Reaction Engineering, 4th edition, Prentice Hall PTR, Upper Saddle River, NJ, 2006.
[44] H. Agrell, M. Birgersson, Boutonnet, Steam reforming of methanol over a Cu/ZnO/Al2O3 catalyst: a kinetic analysis and strategies for suppression of CO formation, J. Power Sources 106 (2002) 249–257.
[45] International Organisation for Standardisation, ISO/TS 14687-2, Hydrogen Fuel-Product Specification—Part 2: Proton exchange membrane Fuel Cell applications for road vehicles; 2012.
[46] M.G. Waller, M.R. Walluk, T.A. Trabold, Performance of high temperature PEM fuel cell materials. Part 1: Effects of temperature, pressure and anode dilution, Int. J. Hydrogen Energy 41 (4) (2016) 2944–2954.
[47] P. Kurra, I. Kasatkin, F. Girgsdies, A. Trunschke, R. Schlögl, T. Ressler, Microstructural characterization of Cu/ZnO/Al2O3 catalysts for methanol steam reforming − a comparative study, Appl. Catal. A: Gen. 348 (2008) 153–164.